Nano Research

Open Access

Research Article

Switchable photoluminescence in hybrid bimetallic halides for solvent-driven erasable information storage applications

Chenliang Li, Yongsheng Sun, Liang Li, and Zhiguo Xia ✉

State Key Laboratory of Luminescent Materials and Devices, Guangdong Provincial Key Laboratory of Fiber Laser Materials and Applied Techniques, Guangdong Engineering Technology Research and Development Center of Special Optical Fiber Materials and Devices, School of Physics and Optoelectronics, South China University of Technology, Guangzhou 510641, China

Cite this article: *Nano Research*, **2026**, *19*, 94908392. https://doi.org/10.26599/NR.2026.94908392

ABSTRACT: The dramatic expansion of data volumes has placed high demands and challenges on optical information technology, and the stimulus-responsive behaviors of luminescent materials have received broad interests therein. Thus, the reliable luminescence materials with fatigue resistance during the storage and erasure process are highly considered. Herein, we design and synthesize organic-inorganic bimetallic halides emitters $Sc(DMSO)_6SbCl_6$ (DMSO = dimethyl sulfoxide), possessing bright yellow-green luminescence with extreme sensitivity to water. Accordingly, a rapid solvent-driven information writing and erasure process is realized. Benefiting from the weak interaction between Sc and O in the hybrid framework, the emission is easily quenched by structural dissociation in water and can be rapidly restored in DMSO in several seconds. Due to its ability to write and erase information through solvent-driven processes, $Sc(DMSO)_6SbCl_6$ exhibits promising potential for storing information. This work offers a new route in the development of hybrid bimetallic halides with switchable emission and erasable information storage.

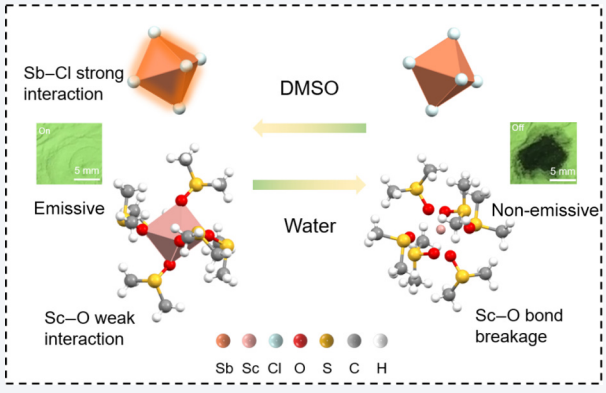

KEYWORDS: bimetallic halides, optical property, switchable luminescence, information storage

1 Introduction

With the rapid development of big data and artificial intelligence technologies, it has created unprecedented demand for efficient, secure, and cost-effective data storage solutions [1, 2]. Amongst, optical information storage technology has received a lot of attention because of its low cost, high capacity, and long lifespan [3–5]. However, its inherent irreversibility poses limitations with regard to repeatable and dynamic encryption [6–8]. To achieve reversible information storage and encryption capabilities, the critical step is the exploitation of optical switching materials exhibiting stimulus-responsive behavior [9]. Currently, traditional optical switches rely on specific wavelengths of light for writing and erasing information [10, 11]. However, optical bleaching in the materials would be induced under high-intensity illumination conditions, significantly compromising their fatigue resistance [12, 13]. Therefore, developing novel optical switches that operate independently of light-driven is essential to overcome these limitations.

Organic-inorganic metal halides (OIMHs) showed great potential in fields of light-emitting diodes, photodetection, and scintillators due to their tunable structures and outstanding optical properties [14–18]. The structural diversity induced by organic molecules endows OIMHs with richly tunable optical properties, making them suitable for new-generation optical information storage materials [19–21]. Notably, the crystal structures in OIMHs often exhibit the properties of "soft lattices" [22–25]. Specifically, the combination of organic and inorganic components tends to occur through weak interactions, such as hydrogen bonds or van der Waals forces [26, 27]. This results in high sensitivity to external chemical environments, such as temperature, humidity, and solvents [28–30]. Based on this, it is advantageous to develop solvent-driven, high-contrast, reproducible stimulus-responsive optical switches by exploiting this sensitivity. For example, Zhang's group developed a methanol-induced structural phase transition in Cu(I)-based OIMHs, enabling a shift in photoluminescence (PL)

Received: December 7, 2025; **Revised:** December 30, 2025
Accepted: December 30, 2025

✉Address correspondence to xiazg@scut.edu.cn

color from cyan to yellow [31]. However, such stimulus-response requires a relatively long response time (150 s), and the contrast of color changes is comparatively poor. Therefore, it is significant to gain solvent-induced PL-switching OIMHs with fast response and high contrast.

Herein, we have successfully synthesized a bimetallic OIMH as $Sc(DMSO)_6SbCl_6$ (DMSO = dimethyl sulfoxide) with rapid reaction at room temperature. In particular, high-quality $Sc(DMSO)_6SbCl_6$ microcrystals can be obtained simply by stirring $ScCl_3$ and $SbCl_3$ raw materials in DMSO at room temperature. Upon excitation by ultraviolet (UV) light, $Sc(DMSO)_6SbCl_6$ exhibits bright yellow-green luminescence. Remarkably, $Sc(DMSO)_6SbCl_6$ exhibited extreme sensitivity to water, showing complete quenching within seconds upon contact with it. It is encouraging that the photoluminescence (PL) performance rapidly recovered under the wetted conditions of the DMSO solvent. The repeatability of the PL switching under solvent-driven conditions was confirmed through structural and optical property measurements, which were attributed to the sensitivity of the Sc–O weak interaction to stimuli. Such excellent solvent sensitivity makes it beneficial for application in fast-response reversible optical information storage. This work provides a novel design strategy for developing fast-response, stimulus-responsive optical switches and opens a new avenue for the next generation of optical information storage materials.

2 Experimental

2.1 Chemicals and materials

$ScCl_3$ was purchased from Leyan (Shanghai, China). $SbCl_3$ and DMSO were obtained from Macklin (Shanghai, China). All chemical reagents were of analytical grade and were used as received.

2.2 Synthesis of $Sc(DMSO)_6SbCl_6$

In a typical synthesis of $Sc(DMSO)_6SbCl_6$ single crystals, 1 mmol $ScCl_3$ and 1 mmol $SbCl_3$ were dissolved in 2 mL DMSO at 95 °C to form a colorless transparent solution. Then the solution was cooled to room temperature slowly. After that, the transparent crystals of $Sc(DMSO)_6SbCl_6$ were filtered off, washed with ethanol to remove the solvent from the crystal surface, and dried in an oven at 60 °C. The obtained single crystals were applied to crystal structure analysis.

$Sc(DMSO)_6SbCl_6$ microcrystals were prepared by stirring 5 mmol $ScCl_3$ and 5 mmol $SbCl_3$ in 8 mL DMSO at room temperature. After about 10 s, the powder exhibited bright yellow-green PL upon the excitation of UV light. The $Sc(DMSO)_6SbCl_6$ microcrystals were also filtered off, washed with ethanol, and dried in an oven at 60 °C. Finally, the crystals were ground into powders for further structural and optical characterization.

2.3 Structural characterization

Single crystal X-ray diffraction (SCXRD) was performed by using an XtaLAB Synergy R X-ray single-crystal diffractometer equipped with a Mo Kα radiation source (λ = 0.71073 Å) at 150 K and a hybrid pixel array detector. The structures were solved by direct methods and refined by full-matrix least-squares techniques on F^2 with SHELX-97. CCDC number 2487869 contains the supplementary crystallographic data for this work. Powder X-ray diffraction (PXRD) patterns of the samples were collected using an Aeris (PANalytical) diffractometer with Cu Kα (λ = 1.541862 Å) radiation operating at 40 kV and 15 mA. Scanning electron microscope images and energy dispersive X-ray spectroscopy (EDS) mapping were taken with a JSM7900F scanning electron microscope from JEOL. X-ray photoelectron spectroscopy (XPS) measurements were performed on an Axis Supra+ X-ray Photoelectron spectroscopy using a monochromatic Al Kα source (15 kV, 20 mA).

2.4 Optical characterization

PL emission, PL excitation (PLE) spectra, and PL decays were recorded on an Edinburgh FLS1000 spectrofluorometer equipped with a continuous xenon lamp (450 W). All the spectral data were recorded at room temperature (RT) unless otherwise noted and corrected for the response of both the spectrometer and the integrating sphere. The temperature-dependent PL spectra were collected by the same spectrophotometer with a heating attachment. Raman spectra were recorded using a Raman spectrometer (Renishaw invia, UK) equipped with a solid-state laser (532 nm).

2.5 Density functional theory (DFT) calculations

DFT calculations were performed by Vienna *ab initio* simulation package (VASP) [32–35]. The interaction between electrons was described by Perdew–Burke–Ernzerhof (PBE) generalized-gradient approximation functional [36, 37]. An energy cutoff of 520 eV and a Monkhorst–Pack k-point grid of 4 × 4 × 4 was applied for all calculations. Convergence criteria for energy and force were set to be less than 10^{-5} eV and 0.01 eV/Å.

3 Results and discussion

3.1 Structural descriptions of $Sc(DMSO)_6SbCl_6$

Highly emissive $Sc(DMSO)_6SbCl_6$ microcrystals were successfully synthesized in macroscopic amounts by simple stirring at room temperature within 1 min (Fig. 1(a)). The weight of the microcrystals synthesized in a single reaction exceeds 3 g, with a chemical yield of 70.8% based on $ScCl_3$ (Fig. S1 in the Electronic Supplementary Material (ESM)). The crystal structure of $Sc(DMSO)_6SbCl_6$ was obtained by resolving single crystal data. The space group of $Sc(DMSO)_6SbCl_6$ was determined as $P\bar{1}$, where a = 9.0735(4) Å, b = 9.3065(4) Å, and c = 9.3987(3) Å (Table S1 in the ESM). The formation of octahedra in the crystal involved the attachment of Sc and Sb atoms to six DMSO molecules, and the attachment of Sc atoms to six Cl atoms, respectively (Figs. 1(b) and 1(c)). The distances between octahedra were much longer than those of the Sc–O and Sb–Cl bond lengths. Thus, their interactions could be neglected, resulting in an isolated zero-dimensional structure. Moreover, the bond length distortion and bond angle were determined as 7.54×10^{-7} and 1.39×10^{-4} from the detailed crystal data, respectively (Tables S2 and S3 in the ESM).

Meanwhile, such microcrystals exhibited a particle size less than 20 μm under observation with a microscope, and they exhibited a yellow-green luminescence under 365 nm UV light (Figs. 1(d) and 1(e)). PXRD pattern of the experimental microcrystals highly agreed with the simulated structure calculated from single-crystal data (Fig. 1(f)). The characteristic peaks of Sb, Sc, Cl, and S were identified. Moreover, XPS was employed to investigate the surface chemical nature of $Sc(DMSO)_6SbCl_6$, resulting in the identification

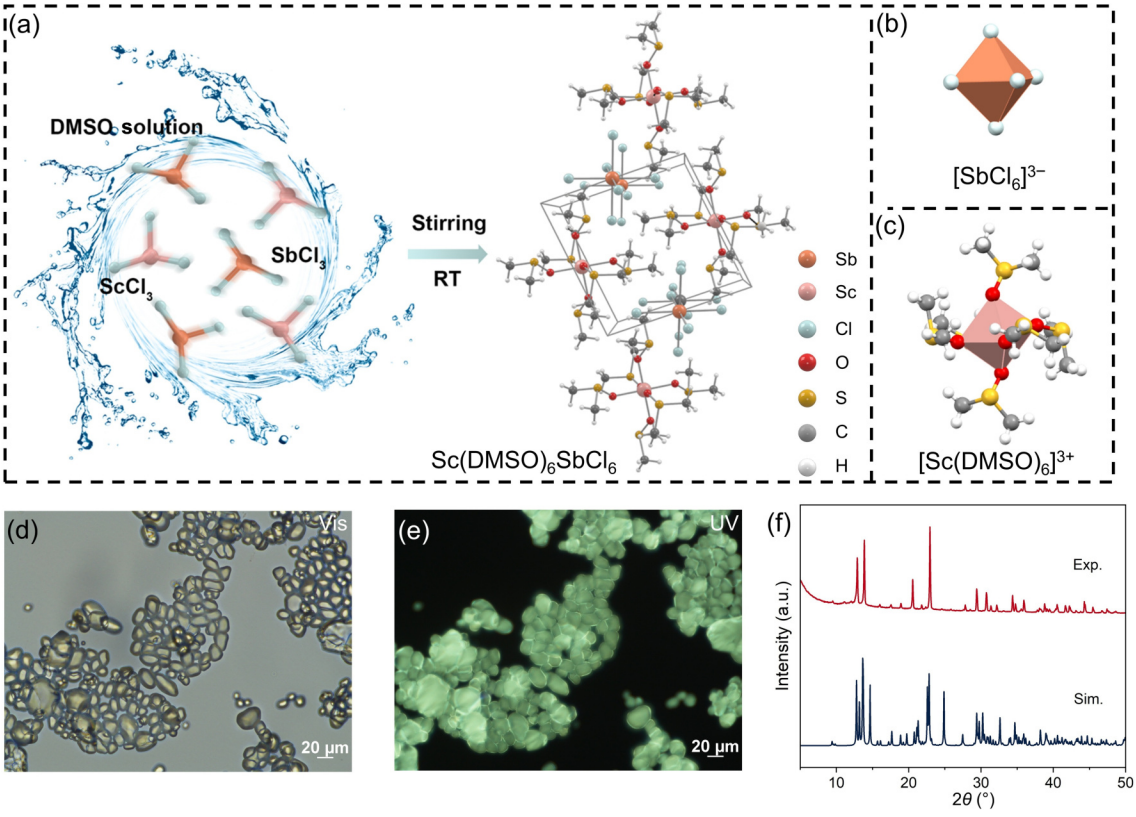

Figure 1 (a) Schematic illustration of rapid room temperature synthesis and single crystal structure of $Sc(DMSO)_6SbCl_6$. Schematic diagram of the structure of (b) $[SbCl_6]^{3-}$ and (c) $[Sc(DMSO)_6]^{3+}$. Micrograph of the $Sc(DMSO)_6SbCl_6$ single crystal under (d) ambient light and (e) UV light. (f) PXRD patterns of $Sc(DMSO)_6SbCl_6$ and simulated pattern from the single crystal.

of characteristic peaks for Sb, Sc, Cl, and S (Fig. S2 in the ESM). SEM-EDS mapping confirmed the uniform distribution of elements Sb, Sc, Cl, and S within the microcrystals (Fig. S3 in the ESM).

3.2 PL properties and mechanism of $Sc(DMSO)_6SbCl_6$

To evaluate the PL properties of $Sc(DMSO)_6SbCl_6$, we measured the PL and PLE spectra at room temperature. Under excitation at 365 nm, $Sc(DMSO)_6SbCl_6$ exhibited broad yellow-green emission peaking at 553 nm with a large Stokes shift of 188 nm and a full width at half maximum (FWHM) of 138 nm (Fig. 2(a) and Fig. S4 in the ESM). Meanwhile, the internal quantum efficiency of $Sc(DMSO)_6SbCl_6$ was determined as 73.69% (Fig. S5 in the ESM). The PL lifetime of $Sc(DMSO)_6SbCl_6$ was determined to be 1.92 μs based on mono-exponential fitting (Fig. 2(b)).

Subsequently, temperature-dependent PL spectra from 80 to 360 K were employed to gain a deep insight into the photophysical mechanism of $Sc(DMSO)_6SbCl_6$. As the temperature rose, there was only a gradual decrease in PL intensity, retaining the single emission peak (Fig. 2(c) and Fig. S6 in the ESM). Concurrently, FWHM will undergo a gradual broadening with rising temperature due to heightened electron–phonon coupling. The temperature dependence of FWHM can derive the Huang–Rhys factor (S) and the phonon energy ($\hbar\omega$) by the following Eq. (1) [38]

$$\mathrm{FWHM}(T) = 2.36\sqrt{S}\hbar\omega\sqrt{\coth\frac{\hbar\omega}{2k_BT}} \quad (1)$$

where k_B is the Boltzmann constant. Therefore, S and $\hbar\omega$ can be identified as 38.25 and 23.7 meV, respectively (Fig. S7 in the ESM). Such a large S value (> 5) indicated a strong electron-phonon coupling in $Sc(DMSO)_6SbCl_6$ [39]. Additionally, we investigated the excitation wavelength-dependent emission spectra with the range of excitation wavelength from 250 to 380 nm. As the excitation wavelength progressively changed, the normalized emission spectra remained essentially unchanged, indicating the single emission source in $Sc(DMSO)_6SbCl_6$ (Fig. S8 in the ESM). These experimental findings confirm that the PL in $Sc(DMSO)_6SbCl_6$ originates from the recombination of self-trapped excitons (STE) within the $[SbCl_6]^{3-}$ octahedron. More specifically, the $^3P_1$ orbital of Sb^{3+} is repelled by the Cl^- ion in the excited state, which leads to a Jahn–Teller–like distortion of the $[SbCl_6]^{3-}$ octahedron [40, 41]. The combination of such distortion and strong electron–phonon coupling results in the generation of STE emission.

Furthermore, first-principles calculations based on density functional theory were performed to gain additional insight into the luminescence mechanism. As shown in Fig. 2(d), $Sc(DMSO)_6SbCl_6$ exhibited a direct bandgap with a bandgap of 2.72 eV. From the diagram of the partial charge density of the valence band maximum (VBM) and the conduction band minimum (CBM), it can be observed that the VBM was mainly composed of Sb and Cl, and the CBM was composed of Sc and organic DMSO (Figs. 2(e) and 2(f)). It is noteworthy that VBM and CBM were composed of $[SbCl_6]^{3-}$ and $[Sc(DMSO)_6]^{3+}$, respectively. Correspondingly, it is difficult for charge transfer from VBM to CBM because isolated octahedra lack overlap. Therefore, the projected density of states (PDOS) showed the CB-2 minimum at 3.45 eV, which is composed of Sb and Cl, played a crucial role in charge transfer (Fig. 2(g)) [42, 43]. These findings proved that the optical properties of $Sc(DMSO)_6SbCl_6$

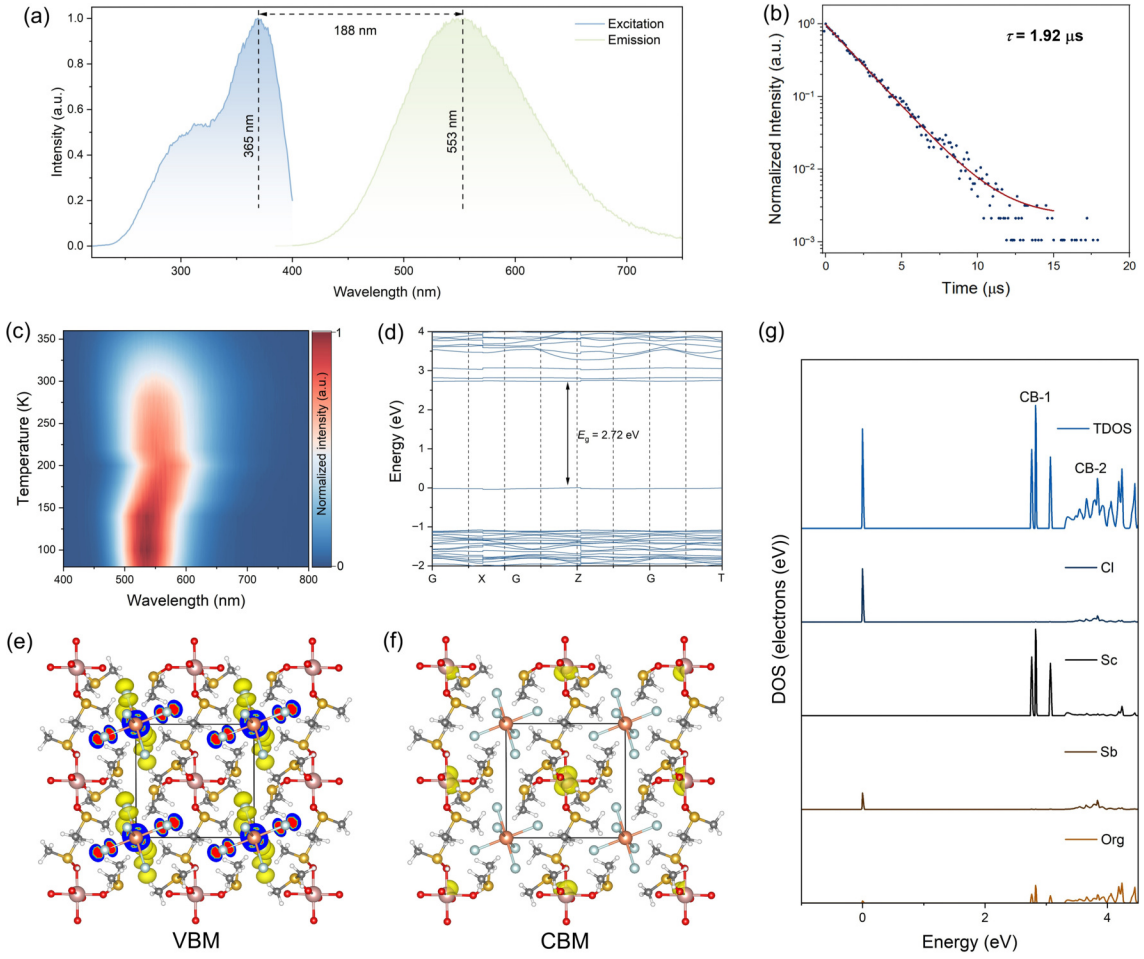

Figure 2 (a) Steady-state PL excitation (left) and PL emission (right) spectra of $Sc(DMSO)_6SbCl_6$. (b) PL decays of $Sc(DMSO)_6SbCl_6$ by monitoring the emission at 553 nm (λ_{ex} = 365 nm). (c) Temperature-dependent emission spectra ranging from 80 to 360 K (λ_{ex} = 365 nm). (d) Calculated band structures of $Sc(DMSO)_6SbCl_6$ based on the DFT method. Diagram of the partial charge density for the (e) VBM and (f) CBM of $Sc(DMSO)_6SbCl_6$ crystal, wherein isosurfaces are electron cloud distributions. (g) Total and partial DOS of $Sc(DMSO)_6SbCl_6$ based on the DFT method.

primarily depend on $[SbCl_6]^{3-}$, and further confirmed that the luminescence originates from the STE emission.

3.3 Solvent stimulus-response properties of $Sc(DMSO)_6SbCl_6$

In contrast to the strong ionic bond between Sb and Cl in $[SbCl_6]^{3-}$, the Sc–O interaction in $[Sc(DMSO)_6]^{3+}$ is relatively weak [44, 45]. It is well known that most OIMHs have poor water stability and are easily quenched by water or water vapor. Such weak interactions enable it to exhibit excellent sensitivity to such external environmental stimuli. We capitalized on this quenching process to create a reversible, solvent-responsive optical switch that relies on the weak interactions between Sc and O (Fig. 3(a)). More specifically, pristine $Sc(DMSO)_6SbCl_6$ exhibited strong PL upon UV excitation, which can be defined as "on". While in the aqueous environment, the PL of $Sc(DMSO)_6SbCl_6$ rapidly quenched, which can be defined as "off". Fortunately, the quenched $Sc(DMSO)_6SbCl_6$-off recovered quickly to the "on" state when placed in a DMSO environment. Figure 3(b) and Video S1 in the ESM documented the process of this rapid transformation.

To shed more light on the mechanism of $Sc(DMSO)_6SbCl_6$ as a stimulus-responsive optical switch, we first employed a situ-PXRD measurement. As shown in Fig. 3(c), the crystalline $Sc(DMSO)_6SbCl_6$ (pristine-on) was found to be in an "off" state after water wetting, with nearly all the diffraction peaks disappearing as it transformed into an amorphous state. Furthermore, when the $Sc(DMSO)_6SbCl_6$-off was immersed in a DMSO environment, all the diffraction peaks were fully recovered (re-on), which is essentially unchanged compared to the pristine state. It is evident that the intrinsic mechanism of $Sc(DMSO)_6SbCl_6$ as stimulus-responsive optical switches involves decomposition and rapid recrystallisation in the presence of water and DMSO. High-resolution XPS of Sc revealed remarkable differences between "on" and "off" states. Both the intensity and peak position of the Sc binding energy have significantly weakened and red-shifted, respectively, signifying a notable change in the coordination environment of Sc on the surface (Fig. 3(d)). Raman spectroscopy was used to analyze the phase transition mechanisms during the transformation process [46]. Following interaction with water molecules, the Raman spectrum of $Sc(DMSO)_6SbCl_6$-off exhibited a significant red shift, reduced intensity, and broadening of the peak in the Sc–O vibrational region (200–600 cm^{-1}). These phenomena collectively suggested that the force constant of the Sc–O bond weakened and the symmetry of its local coordination environment was changed. This is consistent with the disappearance of the PXRD diffraction peaks, confirming the disruption of the crystal structure in water. Concurrently, the intensity of the S=O stretching

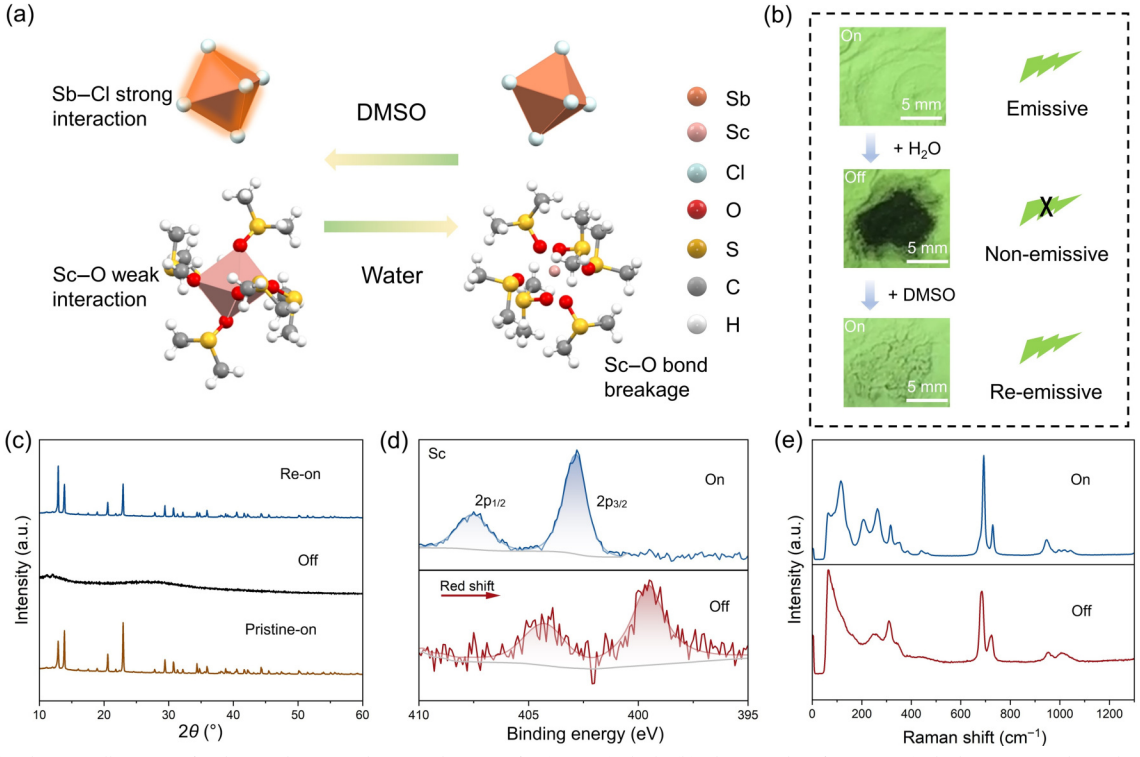

Figure 3 (a) Schematic illustration for the rapid PL Switching mechanism of $Sc(DMSO)_6SbCl_6$. (b) Photographs of $Sc(DMSO)_6SbCl_6$ microcrystal as solvent-driven PL switching (under excitation of 365 nm). (c) Comparison of PXRD patterns of $Sc(DMSO)_6SbCl_6$ in States "pristine-on", "off", and "re-on". Comparison of (d) high-resolution XPS of Sc 2p and (e) Raman spectra of $Sc(DMSO)_6SbCl_6$ in states "off", and "on".

vibration peak at 1050 cm^{-1} increased slightly, representing the formation of free DMSO molecules (Fig. 3(e)) [43].

3.4 Erasable optical information storage application of $Sc(DMSO)_6SbCl_6$

Encouraged by the properties of reversible, solvent-driven optical switches based on $Sc(DMSO)_6SbCl_6$, we applied them further to erasable information storage. Intuitively, we use the presence of PL emission from $Sc(DMSO)_6SbCl_6$ as a binary digit for storing information. In this manner, when PL emission is detected, it is defined as "1"; otherwise, it is defined as "0" (Fig. 4(a)). Combined with American Standard Code for Information Interchange (ASCII) binary logical gates, information storage and retrieval become straightforward (Fig. 4(b)). A proof-of-concept experiment was conducted using a 4 × 8 dot matrix based on $Sc(DMSO)_6SbCl_6$ (Fig. 4(c)). When the initial dot matrix was exposed to ultraviolet light, all the dots displayed as a "1", with no corresponding information being output. Afterwards, some points in the dot matrix were treated with water, after which they were quenched. Consequently, the dot matrix outputs information that is decoded as "SCUT" (Fig. 4(d)). When quenched dots were wetted with DMSO, their luminescence was restored, accompanied by the erasure of information. Repeating the water treatment process after this could produce new output information of "1918", which can also be erased by DMSO. These results illustrate that $Sc(DMSO)_6SbCl_6$ holds significant potential to address the demands in the field of erasable information storage.

4 Conclusion

In summary, we have developed a new class of zero-dimensional organic-inorganic bimetallic halide of $Sc(DMSO)_6SbCl_6$ with simple and rapid synthesis at room temperature, which presents the property of reversible optical switching in response to solvents. Specifically, $Sc(DMSO)_6SbCl_6$ undergoes rapid luminescence quenching when exposed to water, but recovers quickly when placed in a DMSO environment. Based on structural and optical characterization, we infer that this phenomenon originates from a reversible phase transition induced by weak Sc–O interactions under stimulated conditions. Furthermore, we successfully applied $Sc(DMSO)_6SbCl_6$ for information storage with repeatable erase-and-write capabilities. Our work reveals the luminescence switching property of $Sc(DMSO)_6SbCl_6$ for storing and erasing information, demonstrating its significant potential for next-generation optical information storage.

Electronic Supplementary Material: Supplementary material (crystallographic data, supplementary structural, and luminescent properties) is available in the online version of this article at https://doi.org/10.26599/NR.2026.94908392.

Data availability

All data needed to support the conclusions in the paper are presented in the manuscript and the Electronic Supplementary Material. Additional data related to this paper may be requested from the corresponding author upon request.

Acknowledgements

This work is granted by the National Natural Science Foundation of China (No. 22361132525).

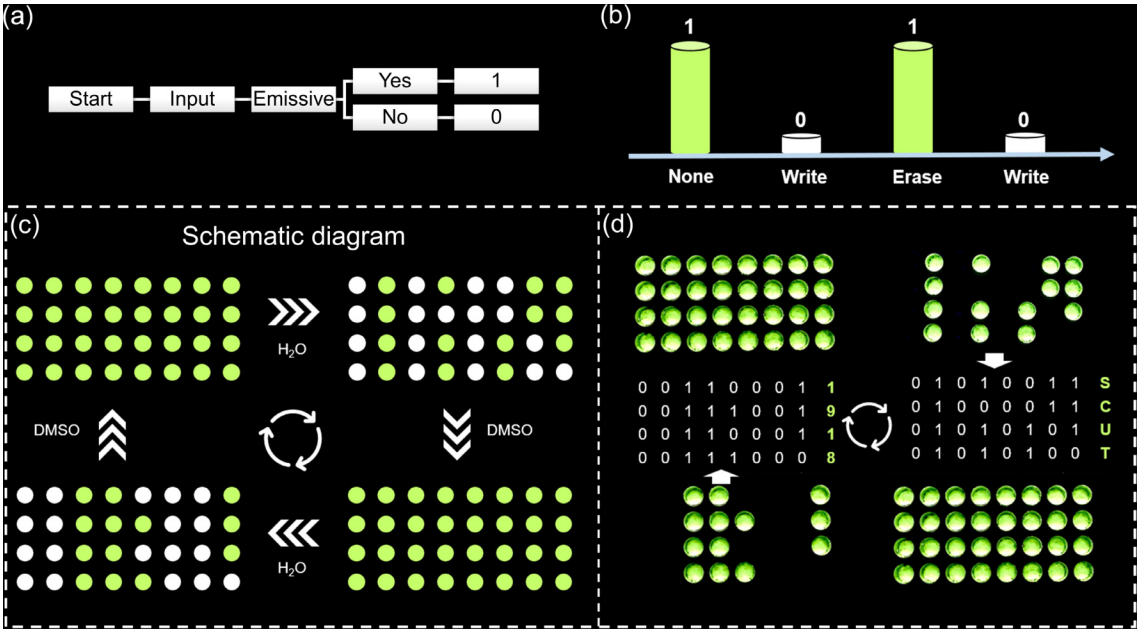

Figure 4 Schematic illustration showing (a) the use of logic gates and (b) write and erase operations based on the PL switch of the $Sc(DMSO)_6SbCl_6$ for information storage. (c) Schematic diagram of a dot matrix for solvent-driven erasable information storage in the proof-of-concept experiment. (d) Photographs based on $Sc(DMSO)_6SbCl_6$ information storage dot matrix, decoded into SCUT and 1918 respectively via ASCII encoding.

Declaration of competing interest

All the contributing authors report no conflicts of interest in this work.

Author contribution statement

C. L. L.: Data curation, project administration, validation, writing manuscript, and experimental design. Y. S. S.: Data curation and experimental design. L. L.: Data curation. Z. G. X.: Project administration, funding acquisition, and revising manuscript. All authors discussed and edited the paper and have approved the final manuscript.

Use of AI statement

None.

References

[1] Zhao, Z. R.; Wang, Z. J.; Shi, Y. Y.; Wan, S.; Li, Z. Y. Multidimensional-encrypted meta-optics storage empowered by diffraction-order decoupling. *Adv. Mater.* **2025**, *37*, 2419322.

[2] Chen, L.; Liu, X. Q.; Liu, F.; Liao, C.; Zhang, L. L.; Zhang, J. H.; Wang, X. J.; Liu, Y. C. Unlocking the potential of up-conversion charging for rapid and high-resolution optical storage with phosphors. *Light: Sci. Appl.* **2025**, *14*, 107.

[3] Sandomirskii, M.; Petrova, E.; Kustov, P.; Chizhov, L.; Larin, A.; Bruyère, S.; Yaroshenko, V.; Ageev, E.; Belov, P.; Zuev, D. Spectral physical unclonable functions: Downscaling randomness with multi-resonant hybrid particles. *Nat. Commun.* **2025**, *16*, 5097.

[4] Zhao, H. P.; Liao, J. Y.; Fu, S. S.; Zi, Y. Z.; Bai, X.; Ci, Y.; Zhang, Y. T.; Cai, X. H.; Li, Y. W.; Cun, Y. et al. Direct 3D lithography of reversible photochromic patterns with tunable luminescence in amorphous transparent media. *ACS Energy Lett.* **2025**, *10*, 1235–1244.

[5] Sun, Y. S.; Zhou, X. Q.; Lun, Z.; Han, K.; Xiong, P. X.; Xia, Z. G. Amorphous to crystalline phase transformation enables tunable persistent luminescence for multi-mode optical information storage. *Adv. Funct. Mater.* **2024**, *34*, 2406336.

[6] Wang, X. Y.; Liu, H. B.; Geng, D. L.; Li, J.; Fan, J. W.; Wu, L. W.; Zhang, Y.; Liu, J. M.; Cui, J.; Lin, J. et al. Nonstoichiometry tailored energy flow pathway toward multicolor dynamic thermo-stimulated luminescence (DTSL) and smart optical information storage. *Laser Photonics Rev.* **2025**, *19*, e01049.

[7] Guan, X. W.; Lei, Z. H.; Yu, X. C.; Lin, C. H.; Huang, J. K.; Huang, C. Y.; Hu, L.; Li, F.; Vinu, A.; Yi, J. B. et al. Low-dimensional metal-halide perovskites as high-performance materials for memory applications. *Small* **2022**, *18*, 2203311.

[8] Wang, L. P.; Tu, D. T.; Li, C. L.; Han, S. Y.; Wen, F.; Yu, S. Q.; Yi, X. D.; Xie, Z.; Chen, X. Y. Engineering trap distribution to achieve multicolor persistent and photostimulated luminescence from ultraviolet to near-infrared II. *Matter* **2023**, *6*, 4261–4273.

[9] Wang, C. R.; Wang, Y. X.; Liu, F.; Yang, B. B.; Shi, T. X.; Chen, L.; Wang, X. J. Security optical memory using multi-stimuli-responsive UV phosphors. *Adv. Opt. Mater.* **2026**, *14*, e02267.

[10] Lin, S. S.; Lin, H.; Huang, Q. M.; Cheng, Y.; Xu, J.; Wang, J. M.; Xiang, X. Q.; Wang, C. Y.; Zhang, L. Q.; Wang, Y. S. A photostimulated $BaSi_2O_5:Eu^{2+},Nd^{3+}$ phosphor-in-glass for erasable-rewritable optical storage medium. *Laser Photonics Rev.* **2019**, *13*, 1900006.

[11] Xiao, D. W.; Huang, X. J.; Cun, Y.; Hu, Z.; Xu, Z.; Bai, X.; Zi, Y. Z.; Fu, L. X.; Haider, A. A.; Qiu, J. B. et al. Large reversible upconversion luminescence modification and 3D optical information storage in femtosecond laser irradiation-subjected photochromic glass. *Sci. China Mater.* **2022**, *65*, 1586–1593.

[12] Ye, Y. L.; Yuan, H. J.; Yang, H. Y.; Mao, Q. N.; Zhao, F. Y.; Ding, Y.; Liu, M. J.; Zhong, J. S. Rewritable optical information storage and dual-channel encryption based on near-infrared enhancement of photostimulated luminescence phosphors. *Laser Photonics Rev.* **2025**, *19*, 2500455.

[13] Tang, B. L.; Zhou, X. Q.; Li, T. R.; Li, L.; Zhang, H. R.; Molokeev, M.; Golovnev, N.; Xia, Z. G.; Lei, B. F. Manipulation of upconversion luminescence in heavily lanthanide-doped halide double perovskites for optical information storage. *Laser Photonics Rev.* **2024**, *18*, 2400468.

[14] Li, T. R.; Tang, B. L.; Jin, J. C.; Han, K.; Zhang, H. R.; Zhao, H. L.; Zhang, X. J.; Molokeev, M.; Wang, Y. Z.; Xia, Z. G. et al. Single

organic cation engineering Cu(I)-based ionic and coordinate type halides as high-efficiency hydrogel scintillator. *Adv. Mater.* **2025**, *37*, e09478.

[15] Han, K.; Zhang, S.; Jin, J. C.; Sun, Y. S.; Wang, Y. Z.; Xia, Z. G. Lattice distortion promoting wavelength-tunable emissions in Cu(I)-based halides for thermography and anti-counterfeiting. *Angew. Chem., Int. Ed.* **2025**, *64*, e202504406.

[16] Zhang, S.; Han, K.; Xia, Z. G. Pseudohalide anions driven structural modulation in distorted tetrahedral manganese(II) hybrids toward tunable green-red emissions. *Angew. Chem., Int. Ed.* **2025**, *64*, e202419333.

[17] Li, C. L.; Tu, D. T.; Liu, Y. H.; Wang, L. P.; Yang, M. J.; Xie, Z.; Yu, S. H.; Xu, J.; Chen, X. Y. Excitation-dependent correlated color temperature manipulation of white-light emission in Sb^{3+}-doped PMA_2ZrCl_6 single crystals. *J. Lumin.* **2024**, *269*, 120513.

[18] Liao, H.R.; Sun, J. X.; Li, W.; Yang, H.; Xie, L. P.; Molokeev, M. S.; Wei, Y.; Xia, F.; Li, G. G. Solvent polarity triggered rapidly reversible quadruple-mode luminescence adjustment in 0D hybrid antimony halides. *Angew. Chem., Int. Ed.* **2025**, *64*, e202515844.

[19] Zhou, L.; Li, K. L.; Chang, Y. Y.; Yao, Y.; Peng, Y. Q.; Li, M.; He, R. X. High-efficiency color-tunable ultralong room-temperature phosphorescence from organic-inorganic metal halides via synergistic inter/intramolecular interactions. *Chem. Sci.* **2024**, *15*, 10046–10055.

[20] Qi, Z. H.; Zhou, B.; Yan, D. P. Recent advances in ultralong room-temperature phosphorescence materials based on metal-organic halides. *Mater. Chem. Front.* **2023**, *7*, 3475–3493.

[21] Li, X. K.; Peng, H.; Xu, O.; Huang, W. J.; Kong, L. H.; Wei, Q. L.; Du, Z. T.; Yang, W. C.; Zou, B. S. Stepwise unlock full-spectrum emission with abnormal anti-thermal quenching in indium-based metal halides by tailoring their crystal structure engineering. *Laser Photonics Rev.* **2025**, *19*, e01270.

[22] Li, C. L.; Wang, L. P.; Tu, D. T.; Shang, X. Y.; Yang, M. J.; Gong, J. C.; Wen, F.; Xing, Y.; Xie, Z.; Jiang, J. X. et al. Luminescence lifetime thermometers based on hybrid cuprous halides with exceptional water resistance and giant thermal expansion. *Light: Sci. Appl.* **2025**, *14*, 224.

[23] Zhao, D. L.; Xiao, G. J.; Liu, Z.; Sui, L. Z.; Yuan, K. J.; Ma, Z. W.; Zou, B. Harvesting cool daylight in hybrid organic-inorganic halides microtubules through the reservation of pressure-induced emission. *Adv. Mater.* **2021**, *33*, 2100323.

[24] Li, L.; Wang, Y. Z.; Jin, J. C.; Han, K.; Zhang, S.; Xia, Z. G. Organic cation methylation design of hybrid Eu(II)-based halide scintillators for improved X-ray detection and imaging. *Adv. Mater.*, **2026**, *38*, e10379.

[25] Zhang, S.; Wang, H.; Wang, Y. L.; Han, K.; Xia, Z. G. Chiral hybrid Cu(I) halide scintillation films with polarization-engineered light management for high-resolution X-ray imaging. *Angew. Chem., Int. Ed.* **2025**, *64*, e202513987.

[26] Lin, J. W.; Wang, P.; Zhou, J. Q.; Mao, L. L. A luminescent hybrid bimetallic halide family with solvent-coordinated rare earth and alkaline earth metals. *Angew. Chem., Int. Ed.* **2024**, *63*, e202400554.

[27] Li, B. H.; Han, K.; Wang, Y. Z.; Sun, Y. S.; Xia, Z. G.; Xu, Y. Mn(II)-based hybrid halide ionogel scintillator film for large-area and high-resolution X-ray imaging. *Angew. Chem., Int. Ed.* **2025**, *64*, e202502440.

[28] Gao, M.; Pan, Y. X.; Lian, H. Z.; Lin, J. Spectral tunability, luminescence enhancement, and temperature sensitivity of Sb^{3+}-doped bismuth-based halide emission crystals for anti-counterfeiting applications. *Inorg. Chem.* **2023**, *62*, 17537–17546.

[29] Jiang, C. Y.; Yan, J.; Du, R. K.; Li, Y.; Wu, M. M.; Xu, B. B.; Qiu, J. R. Stimuli-responsive and defect-regulated luminescent organic metal halide for high-security anti-counterfeiting and force sensing. *Adv. Sci.* **2025**, *12*, e10163.

[30] Fang, S. F.; Zhou, B.; Li, H. X.; Hu, H. L.; Zhong, H. Z.; Li, H. N.; Shi, Y. M. Highly reversible moisture-induced bright self-trapped exciton emissions in a copper-based organic-inorganic hybrid metal halide. *Adv. Opt. Mater.* **2022**, *10*, 2200605.

[31] An, R.; Wang, Q. S.; Liang, Y.; Du, P. Y.; Lei, P. P.; Sun, H. Z.; Wang, X. Y.; Feng, J.; Song, S. Y.; Zhang, H. J. Reversible structural phase transitions in zero-dimensional Cu(I)-based metal halides for dynamically tunable emissions. *Angew. Chem., Int. Ed.* **2025**, *64*, e202413991.

[32] Kresse, G.; Furthmüller, J. Efficiency of *ab-initio* total energy calculations for metals and semiconductors using a plane-wave basis set. *Comput. Mater. Sci.* **1996**, *6*, 15–50.

[33] Kresse, G.; Furthmüller, J. Efficient iterative schemes for *ab initio* total-energy calculations using a plane-wave basis set. *Phys. Rev. B* **1996**, *54*, 11169–11186.

[34] Kresse, G.; Hafner, J. *Ab initio* molecular dynamics for liquid metals. *Phys. Rev. B* **1993**, *47*, 558–561.

[35] Hafner, J. *Ab-initio* simulations of materials using VASP: Density-functional theory and beyond. *J. Comput. Chem.* **2008**, *29*, 2044–2078.

[36] Perdew, J. P.; Burke, K.; Ernzerhof, M. Generalized gradient approximation made simple [Phys. Rev. Lett. 77, 3865 (1996)]. *Phys. Rev. Lett.* **1997**, *78*, 1396.

[37] Perdew, J. P.; Burke, K.; Ernzerhof, M. Generalized gradient approximation made simple. *Phys. Rev. Lett.* **1996**, *77*, 3865–3868.

[38] Zhou, G. J.; Wang, S. D.; Zhang, N.; Mao, Y. L.; Zhou, J.; Xia, Z. G.; Zhang, X. M. Chiral-identified multicolor-tunable photoluminescence via excitation-wavelength modulation in 0D antimony(III) enantiomers for multilevel anti-counterfeiting. *Adv. Funct. Mater.***2026**, *36*, e20933.

[39] Blasse, G.; Grabmaier, B. C. *Luminescent Materials*. Springer: Berlin, 1994.

[40] Li, S. R.; Luo, J. J.; Liu, J.; Tang, J. Self-trapped excitons in all-inorganic halide perovskites: Fundamentals, status, and potential applications. *J. Phys. Chem. Lett.* **2019**, *10*, 1999–2007.

[41] Zhang, Y.; Liu, X. Y.; Sun, H. Y.; Zhang, J. X.; Gao, X. W.; Yang, C.; Li, Q.; Jiang, H.; Wang, J.; Xu, D. S. Strong self-trapped exciton emissions in two-dimensional Na–In halide perovskites triggered by antimony doping. *Angew. Chem., Int. Ed.* **2021**, *60*, 7587–7592.

[42] Lin, H. R.; Zhou, C. K.; Tian, Y.; Siegrist, T.; Ma, B. W. Low-dimensional organometal halide perovskites. *ACS Energy Lett.* **2018**, *3*, 54–62.

[43] Zhang, Y.; Zhang, Y. G.; Zhao, Y. Y.; Jia, H.; Yang, Z. W.; Yin, B. P.; Wu, Y. C.; Yi, Y. P.; Zhang, C.; Yao, J. N. Crystal-liquid-glass transition and near-unity photoluminescence quantum yield in low melting point hybrid metal halides. *J. Am. Chem. Soc.* **2023**, *145*, 12360–12369.

[44] Xu, X.; Ding, Y. X.; Ding, Y.; Xu, F. $[Ga(C_2H_6OS)_6](SbBr_6)$: A highly luminescent organic-inorganic hybrid bimetallic bromide synthesized via a cation hybridization strategy. *Inorg. Chem.* **2025**, *64*, 11335–11341.

[45] Li, Y. Y.; Zhou, Z. C.; Xing, Z. S.; Ko, P. K.; Wong, K. S.; Sung, H. H. Y.; Williams, I. D.; Halpert, J. E. Solvent-induced bright emission in lead-free organic-inorganic antimony bromides with reversible transformation. *Small Methods* **2025**, *9*, 2400003.

[46] Li, B. H.; Sun, Y. S.; Wang, Y. Z.; Jin, J. C.; Han, K.; Xu, Y.; Xia, Z. G. Hybrid Cu(I)-based glassy cluster gel scintillator film by *in situ* UV photopolymerization. *Matter* **2025**, *8*, 102214.